Journal of Advanced Ceramics
2022, **11**(11): 1815–1823
https://doi.org/10.1007/s40145-022-0650-y
ISSN 2226-4108
CN 10-1154/TQ

Research Article

Sintering and mechanical properties of carbon bulks from ordered mesoporous carbon and nano diamond

Bowen MIAO[a,†], Junzhuo WANG[a,†], Jianlin LI[b,*], Shijia GU[a,*], Lianjun WANG[a], Wan JIANG[a,*]

[a] *State Key Laboratory for Modification of Chemical Fibers and Polymer Materials, College of Materials Science and Engineering, Donghua University, Shanghai 201620, China*
[b] *State Key Laboratory of Marine Resource Utilization in South China Sea, School of Materials Science and Engineering, Hainan University, Haikou 570228, China*

Received: February 18, 2022; Revised: July 23, 2022; Accepted: August 23, 2022

Abstract: Powder metallurgy is important in material preparation. Due to the inertness of carbon materials, however, sintering powdered carbon into physically coherent bulks has been a great challenge even at a high temperature (2000 ℃). Improving the sintering activity of carbon powders is the key to the success of the consolidation of the carbon powders. Here ordered mesoporous carbon (OMC) is used as the starting material to produce highly homogeneous novel carbon bulks. During sintering at 1800 ℃, the huge specific surface area of the OMC greatly promotes the migration of carbon atoms and thus the sintering of the OMC by surface diffusion mechanism. When nanodiamond (ND) is added, the volume expansion associated with the phase transformation of diamond to graphite facilitates the densification of the powder compacts. The strong connection between the OMC and the graphite onions derived from the ND bestows the as-prepared carbon bulks with excellent mechanical properties. The current research pioneers a novel way to prepare high-strength carbon materials at relatively low temperatures.

Keywords: mesoporous carbon; nanodiamond (ND); carbon material; high strength

1 Introduction

Thanks to their thermal stability and high-temperature mechanical properties, carbon materials are the most important ultra-high-temperature structural material; they are also widely used in many fields under extreme conditions, e.g., electrical discharge machining, semiconductor manufacturing, and nuclear reactor [1,2]. Conventionally, graphite bulks are fabricated from a mixture of pitch binders (i.e., coal tar or petroleum) and fillers (i.e., coke), shaped via cold isotropic or compression molding, and subjected to subsequent, repeated impregnation and high-temperature (exceeding 2500 ℃) pyrolysis processes [3,4]. However, the above prevailing processes involve huge energy consumption and severe environmental pollution. Sintering the carbon powders into dense bulks directly is a long

† Bowen Miao and Junzhuo Wang contributed equally to this work.
* Corresponding authors.
E-mail: J. Li, jlli@hainanu.edu.cn;
S. Gu, gusj@dhu.edu.cn;
W. Jiang, wanjiang@dhu.edu.cn

alternative, which is, however, extremely difficult due to the inertness of the carbon materials.

There have been many attempts to solve this problem of carbon powder sintering. Generally, the raw powders are vital for the consolidation and mechanical properties of the ceramic materials [5,6], as well as for the carbon materials. Taking an example, carbon nanotubes (CNTs) were used to fabricate the carbon bulks with super properties. After spark plasma sintering (SPS), CNT bulk is composed of randomly distributed CNTs with semi-metallic behavior and good mechanical properties [7]. Additionally, some studies show that nanodiamond (ND) particles can be spark plasma sintered into the graphite onion bulks with a density of 1.3–1.7 g/cm^3 but with super mechanical properties [8,9]. It is believed that the volume expansion associated with the phase change of diamond to graphite contributes to the densification of the bulk graphite or C/C composite bulks, and the graphite onions undergoing this phase change are activated to have higher sintering activity [10–12]. Moreover, the phase change sintering mechanism also has a wide range of applications in boron nitride ceramics [13]. The above studies show that the preparation of the high-performance carbon bulks by the powder metallurgy is promising if the right raw material is used.

Over the past decade, ordered mesoporous carbon (OMC) has been widely studied as a novel form of carbon [14,15]. The OMC has a super specific area with a pore size ranging from 2 to 50 nm, showing the potential for catalysis, energy storage, or conversion [16,17]. In view of the large specific surface areas, OMC powders may be a promising candidate to fabricate the carbon bulks. Ref. [18] shows that transparent high-silica glass can be fabricated from aluminosilicate microporous molecular sieve ZSM-5 powders by the SPS at 1300 ℃; by contrast, the traditional sintering temperature is > 1700 ℃ using the melt-quenched aluminosilicate powders as the raw materials. Similarly, highly transparent (> 90%) silica glass was prepared from mesoporous silica SBA-15 powders at 1020 ℃ [19]. These results indicate that mesoporous materials have high sintering activity and could be consolidated into dense carbon bulks at relatively low temperatures.

Inspired by the above studies, the SPS technology has been successfully used to sinter the OMC powders at 1800 ℃ with a pressure of 80 MPa and a holding time of 5 min. Also, the ND is added to further enhance the mechanical properties of the as-prepared bulk carbon. This paper reports the sintering activity of the OMC that has not been investigated before, providing an insight of the preparation of the bulk carbon with new microstructures.

2 Experimental

2. 1 Fabrication of ND/OMC composite powders

The OMC powders were fabricated via the procedure reported by Wang *et al*. [20]. Briefly, copolymer F127, resol, and ethanol were mixed and stirred for 3 h at room temperature. The obtained homogeneous solution was coated onto polyurethane (PU) foam. When the ethanol evaporated completely from the sample after drying at 25 ℃ for 8 h, the OMC was obtained by heating the dried sample at 100 ℃ for 24 h and post-cured at 150 ℃ for 24 h, before calcined at 700 ℃ for 3 h in N_2. The OMC was ground into fine powders with a size ranging from 3 to 20 μm. Also, the ND powders (Zhengzhou Sino-Crystal Diamond Co., Ltd., China) have a purity of 99.99% and a particle size of 100 nm.

To ensure the repeatability of each run, the total mass of the powders in different proportions was 1 g. A certain amount of the OMC powders were added to ethanol and sonicated for 30 min, and then the ND powders were slowly dispersed into the OMC suspension and sonicated for a further 30 min. The ultrasonic power and frequency were 100 W and 40 kHz, respectively. Finally, the ND/OMC powder suspension was heated to evaporate the solvent under stirring.

2. 2 Preparation of high-strength carbon bulks (HSCBs)

The preparation process of HSCBs is depicted in Fig. 1. The powder mixtures were poured into a graphite die and sintered by an SPS apparatus (Fuji Electronic Industrial Co., Ltd., SPS-725, Japan) in vacuum at 1800 ℃ under a pressure of 80 MPa. The soaking time was 5 min. To explore the effect of ND content on the microstructures and mechanical properties of the bulks, the ND contents were set to 0, 10, 20, 30, 40, and 50 wt%. Also, the as-prepared bulks were denoted as HSCB-0, HSCB-10, HSCB-20, HSCB-30, HSCB-40, and HSCB-50, accordingly.

2. 3 Characterization

The nitrogen adsorption–desorption isotherms were

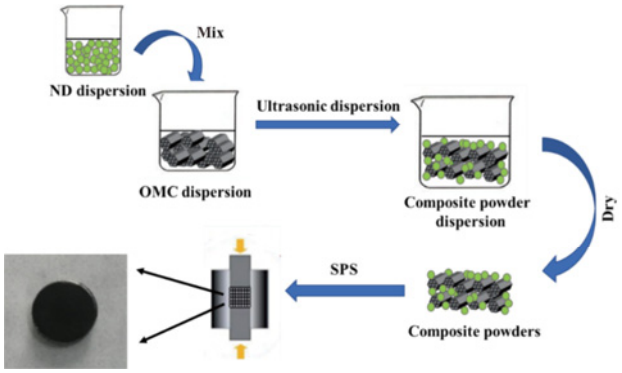

Fig. 1 Schematic of fabrication process for preparing HSCBs.

performed by an automatic high-performance surface area and aperture analyzer (Quantachrome, Autosorb-iQ, USA) to test N_2 adsorption isotherms and pore size distribution of the OMC powders. The bulk densities of the samples were measured by Archimedes method. The microstructures were characterized by a field-emission scanning electron microscope (FESEM; TESCAN, MAIA3, Czech Republic) and a transmission electron microscope (TEM; JOEL, JEM-2100, Japan). The constituent phases were identified by an X-ray diffractometer (Shimadzu, XRD-6000, Japan) with Cu Kα radiation in a scanning range from 15° to 85°. Raman spectra were collected in a spectral range of 500–3000 cm^{-1} at room temperature by a laser Raman confocal micro spectrometer (Renishaw, Via Reflex, UK; 532 nm).

Young's moduli of the HSCBs were measured by an ultrasonic material characterization system (TECLAB, UMS-100, France). Vickers hardness was determined by means of an automatic microhardness testing system (Future Tech, FV-7000, Japan) by indentation method. The bending strength of the sintered bulks (15 mm × 2 mm × 2 mm) was evaluated on an electric universal testing machine (UTM; Shimadzu, AGS-10KNG, Japan) by three-point bending method using Eq. (1):

$$\sigma_b = \frac{3P_bL}{2bh^2} \quad (1)$$

where σ_b is the bending strength of the bulks, P_b is the maximum load, L (= 12 mm) is the span, and b and h represent the width and the height of the bulk samples, respectively. The bending strength was obtained by averaging three measurements for each sample.

3 Results and discussion

3.1 Microstructure evolution of HSCBs

3.1.1 OMC powders

The FESEM micrographs of the powder mixtures and the TEM image of the ND are shown in Fig. S1 in the Electronic Supplementary Material (ESM). In this work, well-dispersed mixed powders were fabricated with the ND powders adsorbed on the surface of the OMC due to the capillary force generated by the evaporation of alcohol. Figure 2 shows the N_2 adsorption–

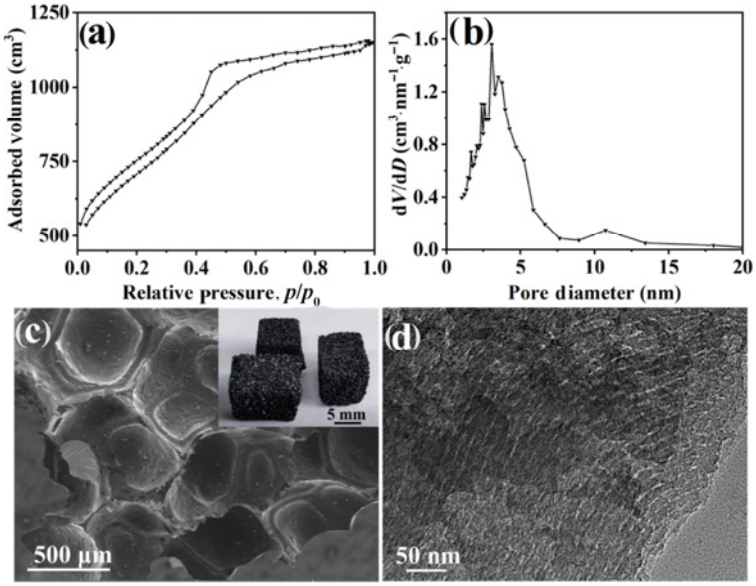

Fig. 2 Characterization of OMC: (a) N_2 adsorption–desorption isotherms, (b) pore size distribution, where V is the pore volume, and D is the pore diameter, (c) FESEM micrograph of OMC porous structure derived from PU foam (the inset is OMC sample), and (d) TEM image of OMC.

desorption isotherms, pore size distribution, FESEM micrograph, and TEM image of the OMC prepared in this work. Typical type-IV isotherms with H1 hysteresis loop at the evident capillary condensation steps are observed, as shown in Fig. 2(a), demonstrating the mesostructure of the OMC with a pore size around 3.0 nm (Fig. 2(b)). Also, as shown in Fig. 2(c), the OMC inherits the PU foam skeleton, which is consistent with Ref. [20]. The high-resolution TEM (HRTEM) image clearly shows the ordered tunnels of the ordered mesostructures of the OMC prepared in this work (Fig. 2(d)).

3.1.2 Phase transformation

Figure 3(a) shows X-ray diffraction (XRD) patterns of the raw powders. The OMC powders exhibit broad diffraction peaks, belonging to typical amorphous carbon. The ND powders have two peaks located at 43.9° and 75.3°, corresponding to the (111) and (220) crystal planes, respectively [21]. After sintering, the diffraction peaks of the OMC become obvious, as shown in Fig. 3(b), indicating that the graphitization of the OMC powders occurs during sintering. Moreover, even if the diamond content reached 50 wt%, the ND phase was not detected in the sample sintered at 1800 ℃. In fact, the diamond core may remain in the graphite onion at 1800 ℃, but the SPS with the self-heating characteristic helps the ND achieve complete phase transition at 1800 ℃.

Raman spectroscopy is a powerful tool to characterize the structural changes of the carbon materials. As shown in Fig. 3(c), the D-band (~1350 cm^{-1}) and G-band (~1580 cm^{-1}) of the OMC powders are highly overlapping, indicating that there are many defects in the OMC [22]. However, the overlap in the Raman spectra of the sintered bulks disappeared (Fig. 3(d)), indicating a reduction in defects and a graphitic transition after sintering, corresponding to the XRD results. The Raman spectra of the raw ND powders (Fig. 3(c)) show a narrow and strong peak at ~1325 cm^{-1}, corresponding to the tensile vibrational mode of the sp^3 hybridized orbital. Also, there is a broadening peak at ~1527 cm^{-1} due to the presence of a portion of non-diamond carbon with functional groups on the surface of the ND particles [23]. In addition, as shown in Fig. 3(d), with the increase in the content of the ND, the value of I_D/I_G is increasing.

3. 2 Densification of HSCBs

A typical shrinkage/sintering curve (i.e., the displacement of the ram in this work) of the OMC powders is shown in Fig. 4(a). The pressure applied to the sample has a significant effect on the consolidation of the powder

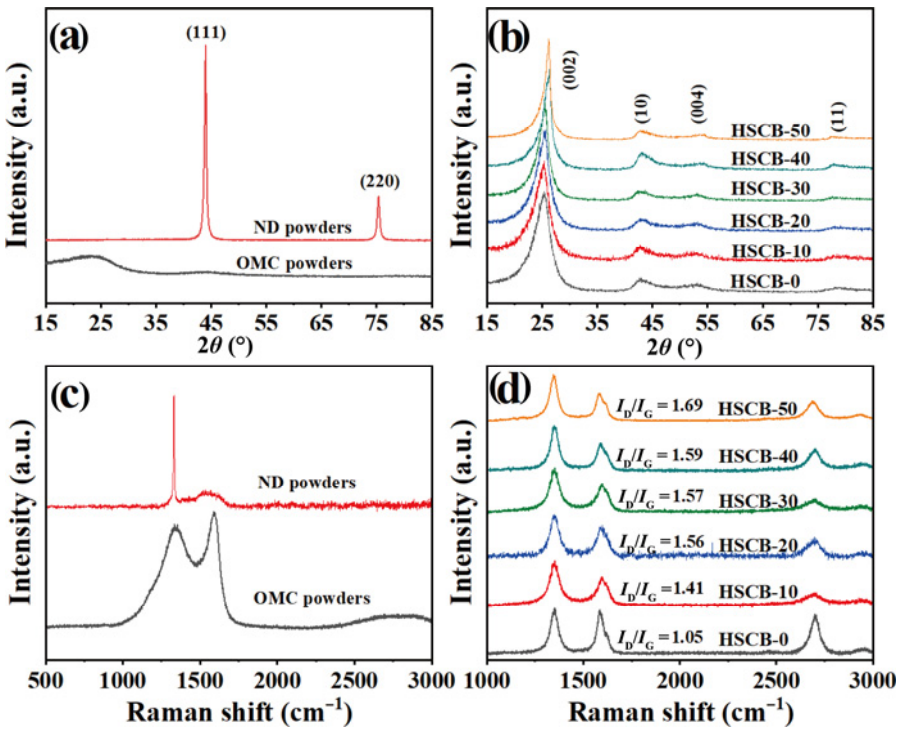

Fig. 3 XRD patterns of (a) raw powders and (b) sintered bulks. Raman spectra of (c) raw powders and (d) sintered bulks , where I_D/I_G is the strength ratio of D-band to G-band.

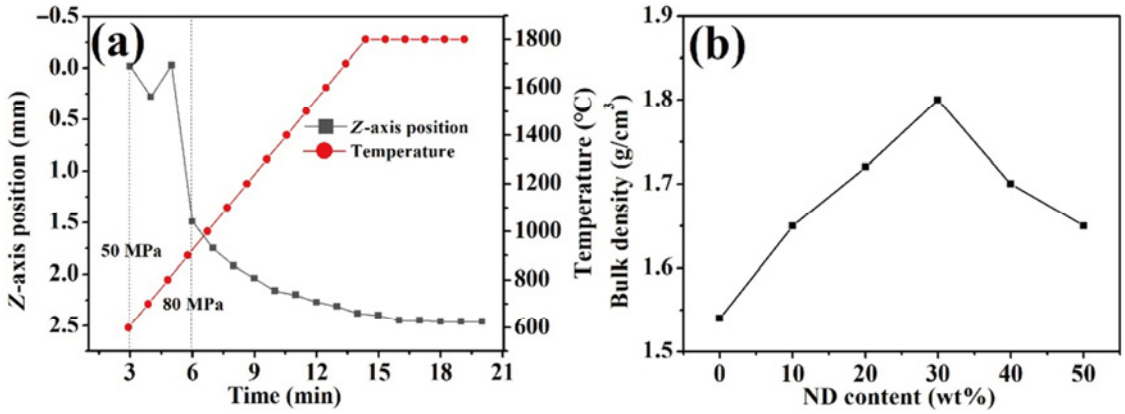

Fig. 4 (a) Typical sintering curve of HSCB-0, and (b) bulk densities of HSCBs.

compact. A steep shrinkage takes place when the pressure increases from 50 to 80 MPa, obviously indicating an increased stacking density associated with the breaking up of the OMC powders. However, this does not mean that the powder compact has become physically coherent. With the temperature increasing, the consolidation of the OMC continues but becomes slow.

The OMC powders are successfully sintered at 1800 ℃, and the obtained HSCB-0 sample has a density of 1.54 g/cm^3, as shown in Fig. 4(b). It is well known that without the binder, the carbon powders are difficult to be consolidated at a temperature as high as 2000 ℃ [24–26], demonstrating the great sintering activity of the OMC. For the carbon materials, the volume diffusion of the carbon atoms at 1800 ℃ is insignificant, that is, the surface diffusion plays a leading role in the mass transport of the sintering process, as demonstrated in Fig. 4(a) that prolonging the holding time at 1800 ℃ does not further densify the compacts. Here Eq. (2) helps elucidate the densification mechanism in this word. This relationship holds when the surface diffusion dominates the mass transportation during sintering.

$$\frac{\Delta S}{S}=\left(\frac{5\gamma\Omega D^*}{RT}\right)^{\frac{2}{5}} r^{-\frac{6}{5}} t^{\frac{2}{5}} \tag{2}$$

where S is the length of the sample, ΔS is the shrinkage of the sample, D^* is the diffusion coefficient, t is the time, r is the particle radius, R is the molar gas constant, T is the temperature, Ω is the void volume, and γ is the surface tension coefficient.

From the viewpoint of sintering, the initial particle size has a very strong influence on the sintering activity; the atom diffusion rate will increase 10^9–10^{12} times when the particle size decreases to the nanoscale [27]. The tunnel structure of the OMC in this work has a wall thickness of 2 nm; therefore, the OMC powders can be reasonably regarded as much fine powders with an extremely small r. The huge surface areas associated with the OMC structure ensure a short diffusing distance for the carbon atoms during the densification process and the rapid migration of the carbon atoms by the surface diffusion mechanism, greatly promoting the densification of the powder compact. Obviously, the fine structure of the OMC makes the pressure applied to the samples more efficiently enhance the densification by, at high temperatures, driving a plastic/viscose flow of mass inside the sample.

As shown in Fig. 4(b), with an ND content of 30 wt%, the density of the bulk reaches 1.80 g/cm^3. It is higher than the density of the graphite onion bulks from the ND [9,10]. This may be attributed to three mechanisms. One is that in this study, the voids between OMC particles are filled out by the ND, increasing the stacking density of the sample. The second mechanism is related to the volume expansion of the change of the ND to graphite in a confined space during the SPS, which facilitates the densification of the powder compact. The third mechanism is that some ND particles pressed into the OMC cause the fragmentation of the OMC powders into even finer particles, which promotes the densification of the powder compact, as shown in Fig. 5.

However, when the content of the ND increases beyond 30 wt%, the density of the carbon bulks starts to decrease. The result is that the graphite onions from the ND particles usually have high strength and form a rigid network inside the sample that hinders the densification, resulting in the reduction in the density, in agreement with Refs. [9,10].

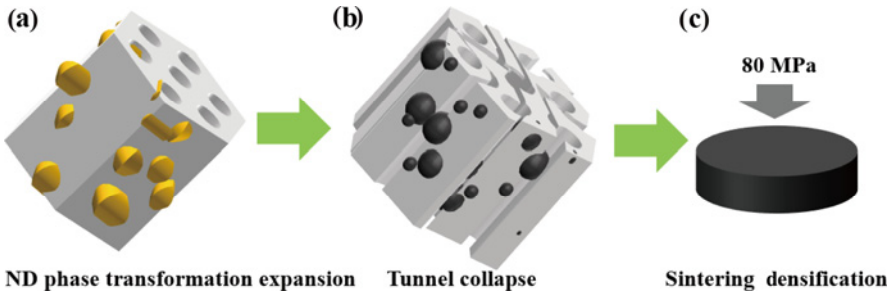

Fig. 5 Schematic diagram of HSCB densification mechanism. ND pierces into OMC channels, causing collapse of OMC and promoting densification of HSCBs.

3. 3 Mechanical properties of HSCBs

Figure 6 shows the microhardness, Young's moduli, and flexural strength of the HSCBs of various ND additions. With the ND contents increasing, the mechanical properties are gradually enhanced, and peak when the ND content is 30 wt%. The bulk density, microhardness, Young's modulus, and flexural strength achieve 1.80 g/cm^3, 0.8 GPa, 18.5 GPa, and 80 MPa, respectively, which are superior or comparable to those of the best commercial carbon materials (Fig. S2 in the ESM). A point to note here is that a strong synergy holds between these mechanical property parameters. The enhancement effect of the present strategy is likely to come from the strong interfacial bonding, similar to the grain boundary strengthening in metal matrix ceramic composites [28], and the TEM results confirm this mechanism. As shown in Fig. 7(a), the sintered OMC is composed of nano fragments of graphite that intertwine with each other. When ND is added, the carbon atoms comprising the outer layers of the onions are activated during the phase transformation, as a result, the nano fragments of OMC are strongly bonded with the graphite onions (Fig. 7(b)). More TEM observations support this statement, as presented in Fig. S3 in the ESM.

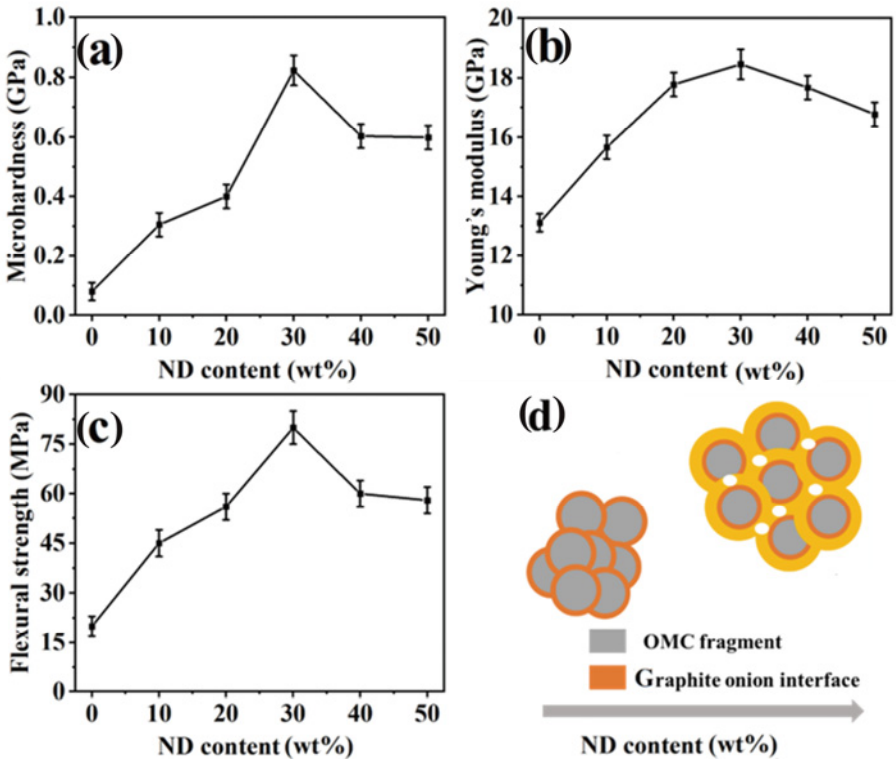

Fig. 6 (a) Microhardness, (b) Young's moduli, and (c) flexural strength of HSCBs with different ND contents; (d) schematic diagram of grain and interface inside the block.

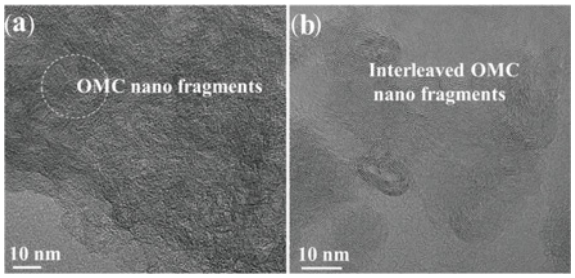

Fig. 7 (a) HRTEM image showing the interweaved OMC nano fragments, and (b) some outer layers of graphite onion tangled with OMC nano fragments.

The strong interfacial bonding can effectively transfer stress and significantly increase the averaged elastic modulus. Therefore, for the improvement of mechanical properties, the density of high-strength interface is very important.

Here, it is reasonable to assume that the grains are uniformly spherical, as shown in Fig. 6(d). When there are N grains, we have obtained the interface area S and volume (V):

$$S = \alpha N\pi(d-\delta)^2 \tag{3}$$

$$V = \frac{4N}{3\beta}\pi d^3 \tag{4}$$

where δ is the interface thickness, $2d$ is the grain size, α is the interface shape factor, and β is the stacking rate.

Then the interface area per unit area is

$$\frac{S}{V} = \frac{3\alpha\beta}{4}\left(\frac{1}{d} - \frac{2\delta}{d^2} + \frac{\delta^2}{d^3}\right) \tag{5}$$

Figure 8 shows that the d increases with the increase of the diamond content. Obviously, when d increases, the area of interface per unit area (S/V) decreases, leading to the decrease of elastic modulus and a significant decrease in mechanical properties. On the other hand, although β is a constant, the size of pores will also increase with the increase of d. The existence of pores will significantly lead to stress concentration, which is another reason for the strength decline.

This phenomenon can be explained by the FESEM micrographs of the fracture surface of the HSCBs (Fig. 8). The smooth fracture surface of HSCB-0 (Fig. 8(a)) indicates that the channels of the OMC have been eliminated, and a highly uniform structure has formed inside the block. With graphite onions incorporated, a granular microstructure forms in the HSCBs, mainly because OMC nano fragments are sintered to graphite onion cores (Fig. 7). The volume of such onion carbon clusters slightly increases as the ND content increases up to 30 wt%, as NDs of low contents are insufficient to wrap the OMC particles. Thus, the increase in the number of interfaces per unit volume causes a significant increase in strength. When the diamond content exceeds 30 wt%, by contrast, the volume of the onion-graphite

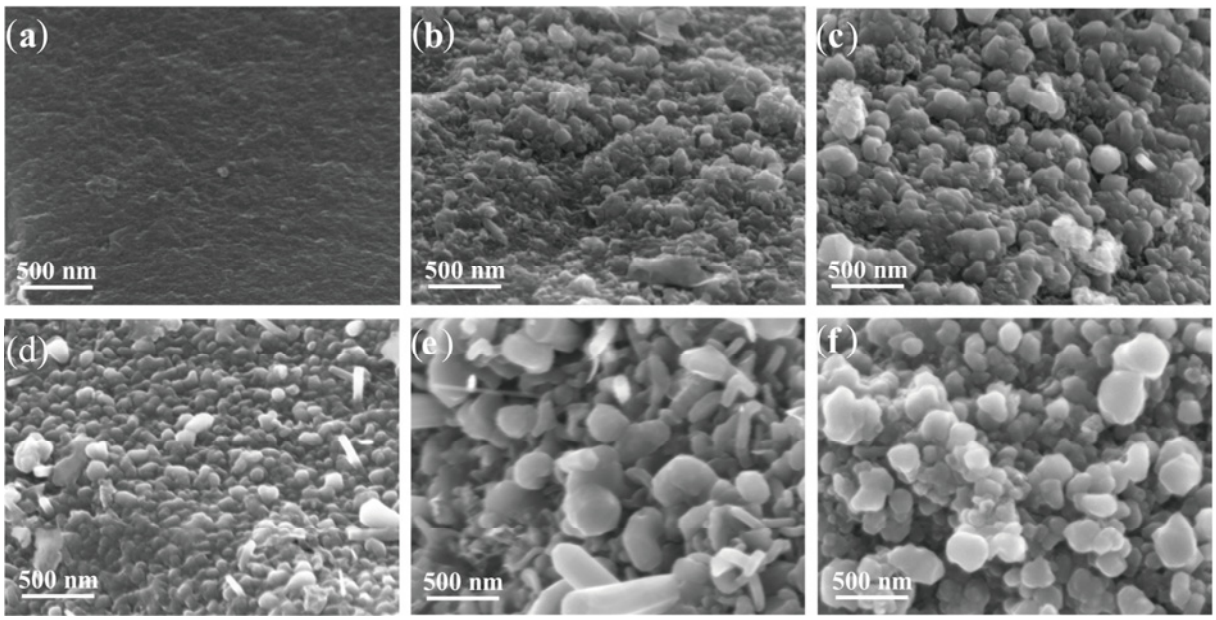

Fig. 8 FESEM micrographs showing the fracture surfaces of (a) HSCB-0, (b) HSCB-10, (c) HSCB-20, (d) HSCB-30, (e) HSCB-40, and (f) HSCB-50.

clusters increases significantly, accompanied by a significant decrease in the density, as depicted by Eq. (5). Much more NDs will form a rigid skeleton and lead to the formation of pores, thus deteriorating the mechanical properties.

4 Conclusions

The OMC proves to be a promising starting material to prepare the HSCBs via powder metallurgy by the SPS. The huge specific surface area enables the sintering of the OMC at relatively low temperatures. The addition of the ND significantly improves the mechanical properties of the as-prepared HSCBs, which are composed of nanographene fragments bonded to graphite onions. With the ND content of 30 wt%, bulk density, microhardness, Young's modulus, and flexural strength of the HSCB-30 achieve 1.80 g/cm^3, 0.8 GPa, 18.5 GPa, and 80 MPa, respectively. This research paves a new way to develop other highly homogeneous nanocrystalline materials for structural and functional applications.

Acknowledgements

This work was supported by the National Natural Science Foundation of China (Nos. 91963204, 52073058, 51871053, and 51962003).

Declaration of competing interest

The authors have no competing interests to declare that are relevant to the content of this article.

Electronic Supplementary Material

Supplementary material is available in the online version of this article at https://doi.org/10.1007/s40145-022-0650-y.

References

[1] Lee SM, Kang DS, Roh JS. Bulk graphite: Materials and manufacturing process. *Carbon Lett* 2015, **16**: 135–146.
[2] Liu ZJ, Guo QG, Shi JL, *et al*. Graphite blocks with high thermal conductivity derived from natural graphite flake. *Carbon* 2008, **46**: 414–421.
[3] Li WJ, Liu Y, Wu GH. Preparation of graphite flakes/Al with preferred orientation and high thermal conductivity by squeeze casting. *Carbon* 2015, **95**: 545–551.
[4] Shen K, Huang ZH, Hu KX, *et al*. Advantages of natural microcrystalline graphite filler over petroleum coke in isotropic graphite preparation. *Carbon* 2015, **90**: 197–206.
[5] Qiu HP, Sun M, Ding HY, *et al*. Study on three dimensional continuous Nicalon-SiC reinforced SiC composites. *Bull Chin Ceramic Soc* 2006, **25**: 63–65. (in Chinese)
[6] Liu ZT, Zhao SQ, Yang T, *et al*. Improvement in mechanical properties in AlN–h-BN composites with high thermal conductivity. *J Adv Ceram* 2021, **10**: 1317–1325.
[7] Li JL, Wang LJ, He T, *et al*. Transport properties of hot-pressed bulk carbon nanotubes compacted by spark plasma sintering. *Carbon* 2009, **47**: 1135–1140.
[8] Ukhina AV, Dudina DV, Anisimov AG, *et al*. Porous electrically conductive materials produced by Spark Plasma Sintering and hot pressing of nanodiamonds. *Ceram Int* 2015, **41**: 12459–12463.
[9] Ran JJ, Lin KP, Yang HT, *et al*. A new family of carbon materials with exceptional mechanical properties. *Appl Phys A* 2018, **124**: 262.
[10] Lin KP, Fang HL, Gao A, *et al*. Nanoburl graphites. *Adv Mater* 2021, **33**: 2007513.
[11] Li ZJ, Lin KP, Fang HL, *et al*. The mortise and tenon structure enabling lamellar carbon composites of ultra-high bending strength. *J Mater Sci Technol* 2023, **133**: 249–258.
[12] Lin KP, Fang HL, Wen F, *et al*. Ultra-strong nanographite bulks based on a unique carbon nanotube linked graphite onions structure. *Carbon* 2019, **149**: 436–444.
[13] Yang HT, Fang HL, Yu H, *et al*. Low temperature self-densification of high strength bulk hexagonal boron nitride. *Nat Commun* 2019, **10**: 854.
[14] Fang Y, Gu D, Zou Y, *et al*. A low-concentration hydrothermal synthesis of biocompatible ordered mesoporous carbon nanospheres with tunable and uniform size. *Angew Chem Int Ed* 2010, **49**: 7981–7991.
[15] Xue CF, Tu B, Zhao DY. Evaporation-induced coating and self-assembly of ordered mesoporous carbon–silica composite monoliths with macroporous architecture on polyurethane foams. *Adv Funct Mater* 2008, **18**: 3914–3921.
[16] Benzigar MR, Talapaneni SN, Joseph S, *et al*. Recent advances in functionalized micro and mesoporous carbon materials: Synthesis and applications. *Chem Soc Rev* 2018, **47**: 2680–2721.
[17] Cha YH, Hong KS, Lee SC, *et al*. Synthesis and photophysical properties of erbium-included mesoporous materials for optical amplification. *J Nonlinear Opt Phys* 2004, **13**: 497–501.
[18] Wang LJ, Jiang W, Chen LD, *et al*. Formation of a unique glass by spark plasma sintering of a zeolite. *J Mater Res* 2009, **24**: 3241–3245.
[19] Zhang X, Yu XW, Zhou BY, *et al*. Sinterability enhancement by collapse of mesoporous structure of SBA-15 in fabrication of highly transparent silica glass. *J Am Ceram Soc* 2015, **98**: 1056–1059.

[20] Wang JX, Xue CF, Lv YY, *et al*. Kilogram-scale synthesis of ordered mesoporous carbons and their electrochemical performance. *Carbon* 2011, **49**: 4580–4588.
[21] Zou Q, Li YG, Zou LH, *et al*. Characterization of structures and surface states of the nanodiamond synthesized by detonation. *Mater Charact* 2009, **60**: 1257–1262.
[22] Obraztsova ED, Fujii M, Hayashi S, *et al*. Raman identification of onion-like carbon. *Carbon* 1998, **36**: 821–826.
[23] Ferrari AC, Robertson J. Raman spectroscopy of amorphous, nanostructured, diamond-like carbon, and nanodiamond. *Philos Trans Roy Soc A Math Phys Eng Sci* 2004, **362**: 2477–2512.
[24] Lin QY, Li TQ, Liu ZJ, *et al*. High-resolution TEM observations of isolated rhombohedral crystallites in graphite blocks. *Carbon* 2012, **50**: 2369–2371.
[25] Zhao Y, Liu ZJ, Wang HQ, *et al*. Microstructure and thermal/mechanical properties of short carbon fiber-reinforced natural graphite flake composites with mesophase pitch as the binder. *Carbon* 2013, **53**: 313–320.
[26] Zhao Y, Shi JL, Wang HQ, *et al*. A sandwich structure graphite block with excellent thermal and mechanical properties reinforced by *in situ* grown carbon nanotubes. *Carbon* 2013, **51**: 427–430.
[27] Lu K. Sintering of nanoceramics. *Int Mater Rev* 2008, **53**: 21–38.
[28] Lu K, Lu L, Suresh S. Strengthening materials by engineering coherent internal boundaries at the nanoscale. *Science* 2009, **324**: 349–352.